Available online at www.sciencedirect.com
SCIENCE DIRECT®
Journal of Nuclear Materials 329–333 (2004) 289–293
journal of nuclear materials
www.elsevier.com/locate/jnucmat

SANS investigation of proton-irradiated EUROFER97

P. Spätig [a,*], R. Schäublin [a], N. Baluc [a], J. Kohlbrecher [b], M. Victoria [a]

[a] Fusion Technology Materials CRPP-EPFL, Association EURATOM–Confederation Suisse, 5232 Villigen PSI, Switzerland
[b] ASQ – Paul Scherrer Institute, CH-5232 Villigen PSI, Switzerland

Abstract

Small angle neutron scattering experiments have been undertaken on the tempered martensitic steel EUROFER97 after proton irradiation at 250 and 350 °C and for doses of 0.3 and 1 dpa. It has been qualitatively shown that the scattering arises from distributions of irradiation-induced defects that peak below one nanometer in size (radius). The number density in the distribution increases with dose for each irradiation temperature. At the same dose, the density of the defects has been found much larger after irradiation at 250 °C than after 350 °C. The variation of ratio between the nuclear and magnetic scattering with dose suggests that the chemical composition of the nano-defects or helium content in the nano-bubbles is dose dependent.

1. Introduction

Nano-scale irradiation-induced defects are believed to significantly contribute to the irradiation-hardening in metals along with the microscopic defects. Transmission electron microscopy (TEM) allows direct observations of defects whose size is larger than about 1 nm in weak beam imaging. Other techniques have to be used to reveal ultra-fine scale microstructures. It is well established that small angle neutron scattering (SANS) is an effective technique to characterize nano-scale distributions of features in terms of number density, size distribution and chemical composition. A number of studies have been recently undertaken to characterize the composition of irradiation-induced precipitates in reactor pressure vessel steels [1], to investigate helium bubbles in the 9% Cr martensitic steels [2], or to study the irradiation-enhanced precipitation of Cr-rich precipitates in the 7–12% Cr martensitic steels [3] for example.

The 7–12% Cr tempered martensitic steels are candidate materials for structural applications in fusion reactors and in advanced high temperature fission reactors [4]. Below an irradiation temperature of about 450 °C, irradiation-hardening is important even at low doses (<1 dpa) [5]. Further, fusion neutrons will generate gaseous impurities – helium and hydrogen – that form bubbles whose contribution to the deterioration of the mechanical properties depends on temperature and is not yet fully understood [6]. Hence, it is of primary importance to identify the whole set of defects produced by irradiation like bubbles, voids, precipitates, dislocation loops and so on, from the nanoscopic to the microscopic scale. By using the SANS technique, the goal of this investigation was to characterize the nanoscopic feature distributions that form under proton irradiation in the tempered martensitic steel EUROFR97 as a function of dose and irradiation temperature.

2. Experimental procedure

The alloy in this study is the reduced activation EUROFER97 steel, heat E83697, produced by Böhler AG. This steel contains 8.90 wt% Cr, 0.12 wt% C, 0.46 wt% Mn, 1.07 wt% W, 0.2 wt% V, 0.15 wt% Ta, and Fe for the balance. The steel was heat-treated by normalizing at 1253 K for 0.5 h and tempering at 1033 K for 1.5 h. The steel was fully martensitic after quenching.

* Corresponding author. Tel.: +41-56 310 29 34; fax: +41-56 310 45 29.
E-mail address: philippe.spatig@psi.ch (P. Spätig).

0022-3115/$ - see front matter © 2004 Elsevier B.V. All rights reserved.
doi:10.1016/j.jnucmat.2004.04.052

Small flat tensile specimens, with a 5.5 mm gauge length, 2.5 mm wide and 0.3 mm thick, were used to carry out the SANS measurements. The specimens were irradiated with the 590 MeV proton irradiation facility PIREX located at the Paul Scherrer Institute – Switzerland. Details about the irradiation facility can be found in [7]. Irradiations up to 0.3 and 1 dpa were performed at temperatures of 250 and 350 °C. Note that with protons of 590 MeV, the helium production rate in the tempered martensitic steel is about 100 appm He/dpa.

The SANS measurements were also carried out at the Paul Scherrer Institute. Neutron scattered intensities were obtained with a neutron wavelength of 0.5 nm and a specimen–detector distance of 2 m, which allows measurement over a range of q from 0.35 to 2.6 nm^{-1}, with q being the scattering vector. The measurements were performed in a strong saturating magnetic field perpendicular to the incident neutron beam. The raw data counts on the detector were corrected by subtracting off the background, the parasitic scattering and the scattered intensity of a unirradiated specimen. Finally, the anisotropy of the detector was accounted for by normalizing the corrected scattered signal with the measurement obtained from a water reference specimen with a known isotropic cross-section.

In order to characterize the distribution of irradiation-induced scattering features, we use the equation relating the differential coherent small angle cross-section, $d\Sigma/d\Omega$, which is proportional to the scattered intensity, to a dilute distribution of a single type of scattering features, with the following equation [8]:

$$\frac{d\Sigma}{d\Omega}(q) = \Delta\rho^2 \int N(R) V_p^2(R) P(q,R)\, dR, \tag{1}$$

where $N(R)\,dR$ is the number of particles per unit volume having a diameter between R and $R + dR$, $V_p(R)$ is the volume of a particle and $P(q,R)$ is the form factor of the particles. $\Delta\rho^2$ is the difference between the scattering length density of the particle and that of the matrix; $\rho = b/\Omega_a$ with b being the average scattering length and Ω_a the corresponding average atomic volume. $\Delta\rho^2$ is the so-called contrast. $d\Sigma/d\Omega$ is proportional to the corrected scattered intensity. In the following, we present the corrected scattered intensities so all the results in this contribution must be considered *qualitative*. When a saturating magnetic field (horizontal and perpendicular to the beam) is applied, the coherent small angle neutron scattering arises from variations in the scattering length density in nuclear contrast as well as in magnetic contrast so that

$$\Delta\rho^2 = \Delta\rho_n^2 + \Delta\rho_m^2 \sin^2(\phi), \tag{2}$$

where ϕ is the angle between the applied magnetic field direction and the projected observation direction onto the plane perpendicular to the neutron beam. In the case of nano-voids or nano He bubbles, $\Delta\rho_n$ and $\Delta\rho_m$ can be written as

$$\Delta\rho_n = \frac{b_n^{matrix}}{\Omega^{matrix}} \quad \text{for voids}$$

$$\Delta\rho_n = \frac{b_n^{matrix}}{\Omega^{matrix}} - \frac{b^{He}}{\Omega^{He}} \quad \text{for He-bubbles,} \tag{3a}$$

$$\Delta\rho_m = \frac{b_m^{matrix}}{\Omega^{matrix}} \quad \text{for voids and He bubbles.} \tag{3b}$$

The general equation for the differential cross-section in the case of a magnetic plus nuclear scattering can then be written

$$\frac{d\Sigma_{tot}}{d\Omega}(q,\phi) = \frac{d\Sigma_{Nucl}}{d\Omega}(q) + \frac{d\Sigma_{Mag}}{d\Omega}(q)\sin^2(\phi). \tag{4}$$

For a given q, Eq. (4) allows splitting of the scattering patterns into a nuclear and a magnetic component by choosing $\sin^2(\phi)$ as the independent variable.

3. Results and discussion

The scattering cross-sections of the specimens irradiated at 250 °C at the two doses of 0.3 and 1 dpa are presented in Fig. 1(a) as a function of q along with that of the unirradiated reference specimen. The cross-sections are presented in arbitrary units and have been determined in a 10° wide vertical sector, centered at 90° from the magnetic field direction, where the scattered intensity is maximal. The additional scattered intensity arising from the irradiation-induced defect microstructure becomes detectable for q values larger than 0.7 nm^{-1}. Note that the scattered intensity for the specimen irradiated up to 1 dpa is clearly larger than that of the specimen irradiated at 0.3 dpa. For the sake of clarity, only the scattered intensity of the specimen irradiated at 350 °C and 1 dpa is shown in Fig. 1(b). It is worth noting that the amplitude of the scattered intensity after 1 dpa is much weaker than that of the specimen irradiated at 250 °C to the same dose. Actually, the same observation holds for the specimens irradiated to 0.3 dpa. A variety of small irradiation-induced defect clusters may contribute to the scattered intensity; these include nanometer-sized voids and helium bubbles, and small dislocation loops. Note that at the doses under investigation, transmission electron microscopy observations show defects that are not clearly identified and are referred to as black dots. Those might be small precipitates or dislocation loops. As shown in [9], the contribution of dislocation loops to the SANS signal can be considered negligible. Thus, the SANS signal arises from features that may be either small irradiated-induced precipitates, nanometer-sized voids or helium

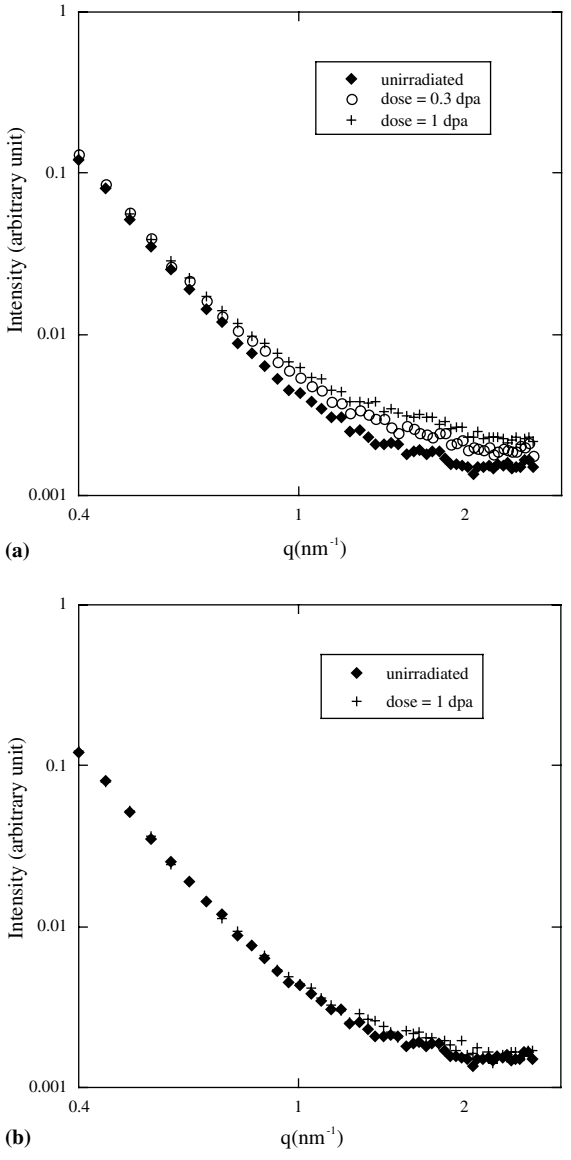

Fig. 1. (a) Scattered intensities after irradiation at $T = 250$ °C, for doses of 0.3 and 1 dpa, along with the scattered intensity of a unirradiated specimen. (b) Scattered intensity after irradiation at $T = 350$ °C, for a dose of 1 dpa, along with the scattered intensity of a unirradiated specimen.

bubbles. In the following and in order to proceed with a qualitative discussion, we assume that we deal with a single distribution of spherical nano-features. This last assumption constitutes a simplification of the more complex real distribution of different types of nanometer-sized defects but allows assessment of the general trend of the evolution of the nano-feature defect distribution with dose and irradiation temperature. We recall that the distribution function is reflected in Eq. (1) by $N(R)$. The log-normal function is used for the distribution which is written as

$$N(R) = \frac{N}{\sqrt{2}\pi s R} \exp\left(-\frac{(\log(R/R_o))^2}{2s^2}\right), \quad (5)$$

where R_o and s are the so-called scale and shape parameters and N is the number density. In order to better assess the evolution trend of N and R_o with irradiation dose and irradiation temperature, a value of 0.2 for s was selected. The implications of using a fixed value for s are discussed at the end of this section.

With the previous assumptions, it has been possible to satisfactorily fit the scattered intensities of the irradiated specimens by adjusting two parameters of the log-normal distribution function, namely R_o and N. The distribution functions obtained are plotted in Fig. 2, where it can be seen that all the distributions peak below 1 nm. Due to the non-uniqueness in the fitted parameters (see last paragraph of this section), the slight variations in the position of the peak at the different doses and irradiation temperatures are not necessarily representative of a specific physical mechanism of the defect accumulation. Interestingly, the number density at a given irradiation temperature increases with dose but the number densities after the irradiations at 350 °C are much lower than those at 250 °C. The dose dependence of N for the two irradiation temperatures is indicated in Fig. 3. Clearly, the sub-nanometer irradiation-induced defects tend to disappear with increasing irradiation temperature by enhanced recombination of point defects and possible coarsening of the clusters. It is also important to emphasize that the features described by these distributions have a size well below the TEM resolution limit.

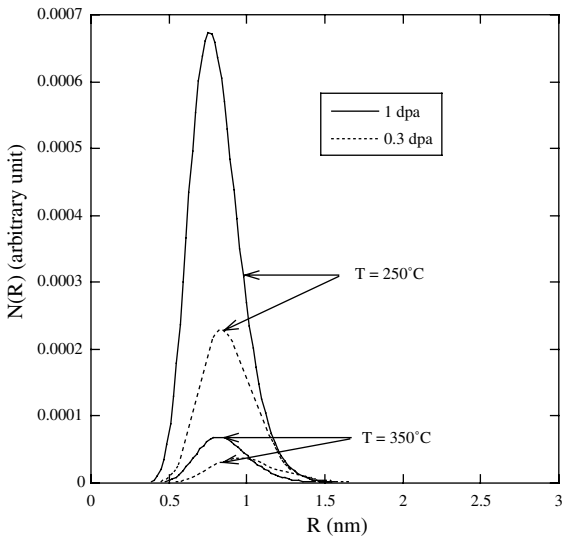

Fig. 2. Size distribution of the scattering features for the different irradiation conditions investigated.

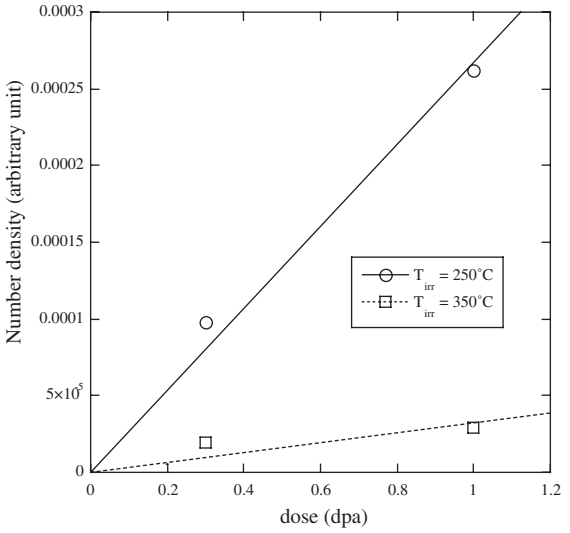

Fig. 3. Number density N as a function of dose for the two irradiation temperatures.

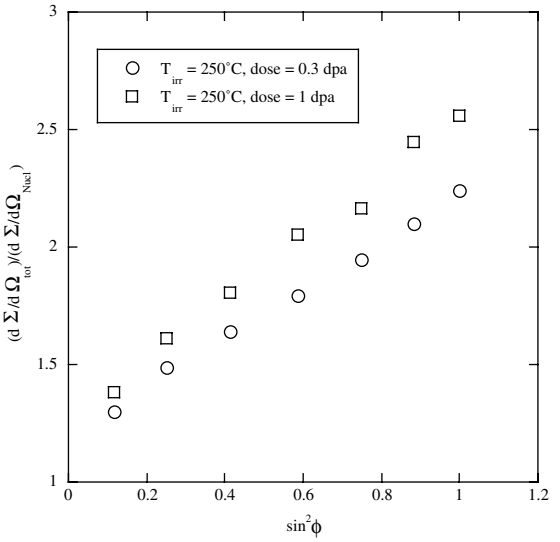

Fig. 4. $(d\Sigma_{tot}/d\Omega)/(d\Sigma/d\Omega_n)$ ratio as a function of $\sin^2\phi$.

It is possible to get additional information about the chemical composition of the scattering features by splitting the magnetic and nuclear cross-sections. It was found that between $q = 0.03\ \mathrm{nm}^{-1}$ and $q = 1\ \mathrm{nm}^{-1}$ the η ratio, defined as $(d\Sigma_{tot}/d\Omega)/(d\Sigma/d\Omega_n)$, does not depend on q. Assuming that the scattering features are helium bubbles for example, the ratio η, which depends on the angle ϕ, can be written as a function of the contrast as

$$\eta = 1 + \left(\frac{b_m^{matrix}/\Omega^{matrix}}{b_n^{matrix}/\Omega^{matrix} - b^{He}/\Omega^{He}} \right)^2 \sin^2(\phi). \qquad (6)$$

The ratio η, which is equal to $(d\Sigma_{tot}/d\Omega)/(d\Sigma/d\Omega_n)$, was determined in the case of the irradiation at 250 °C for the two doses by averaging the scattered intensity over sectors of 10° width. In Fig. 4, we plot $(d\Sigma_{tot}/d\Omega)/(d\Sigma/d\Omega_n)$ against $\sin^2\phi$ where a slight increase of the slope is observed with increasing dose. In case of helium bubbles, this suggests that the atomic volume Ω^{He} of the He atoms trapped inside the bubbles varies or in other words that the amount of helium trapped is dose dependent.

Let us finally emphasize that the revealed sub-nanometer irradiation-induced defects have to be taken into account in modeling the irradiation-hardening. In [10], we showed that irradiation-hardening cannot be satisfactorily described by the dispersed barrier model by taking into account only the density of visible defects by TEM. Thus, the contribution of nano-scale features characterized in this study needs to be incorporated in a model of irradiation-hardening. The key parameter to be used would be the interparticle spacing L that can be calculated with the following equation [11]:

$$L = \left[\int DN(R)\,dR \right]^{-1/2} = \left[\int 2RN(R)\,dR \right]^{-1/2}, \qquad (7)$$

where D is the diameter of the particles. Clearly L is dependent on the distribution function $N(R)$. We recall that the shape parameter s of the presented distributions was not fitted but that a fixed value of 0.2 was chosen. Three parameter fits were also performed and it was observed, on one hand, that the fitted value of s falls in the range 0.1–0.3 and, on the other hand, that various sets of three parameters (N, R_o,s) can yield good fitting. However, even if different distributions are possible, all of them peak below 1 nm. L was calculated for three distribution functions $N(R)$ obtained, respectively, with $s = 0.1$, 0.2 and 0.3 and it was found that the uncertainty on s yields an error bar on L of maximum 30%. The interparticle spacing remains comparable independently of the distribution used and the associated error bar is of the same order of the one that we would expected on the α constant characterizing the strength of the obstacle in the Orowan's equation [11]. Finally, we note that using another distribution function like the normal distribution affects only little the mean interparticle spacing.

4. Summary

Specimens of the tempered martensitic steel EUROFER97 have been irradiated with 590 MeV protons at 250 and 350 °C and two doses, 0.3 and 1 dpa. While at these doses only few irradiation-induced defects that cannot be clearly identified, are detected by electron transmission microscopy, it has been shown that small-angle neutron scattering permits identification of nano-

scale features, responsible for the additional scattered intensity by the irradiated specimens. It has been found that their number density increases with the dose and that it is much larger at 250 °C than at 350 °C. While the SANS signals have been fitted with a single distribution of spherical features, it is believed that this simplified analysis shows the correct trend of the evolution of the nano-defect distribution with dose and temperature. Finally, the evolution with dose of the ratio between the nuclear and magnetic contrast suggests that the chemical composition of the features depends on the dose.

Acknowledgements

The financial support of the Swiss National Foundation and of EURATOM is gratefully acknowledged. This work is based on experiments performed at the Proton Accelerator and Hot Laboratory, Paul Scherrer Institute, Villigen, Switzerland.

References

[1] G.R. Odette, C.L. Liu, B.D. Wirth, Microstructure evolution during irradiation, in: I.M. Robertson, G.S. Was, L.W. Hobbs, T. Diaz de la Rubia (Eds.), MRS Symposium 439, 1997, p. 457.
[2] R. Coppola, M. Magnani, R. May, A. Moeslang, J. Appl. Crystallogr. 33 (2000) 469.
[3] M.H. Mathon, Y. de Carlan, G. geoffroy, X. Averty, A. Alamo, C.H. de Novion, J. Nucl. Mater. 312 (2003) 236.
[4] R.L. Klueh, D.R. Harries, ASTM Monograph 3, American Society for Testing and Materials, West Conshohocken, PA, 2001.
[5] P. Spätig, R. Schäublin, S. Gyger, M. Victoria, J. Nucl. Mater. 258–263 (1998) 1345.
[6] H. Trinkaus, B.N. Singh, J. Nucl. Mater. 323 (2003) 229.
[7] P. Marmy, M. Daum, D. Gavillet, S. Green, W.V. Green, F. Hegedüs, S. Proennecke, U. Rohrer, U. Stiefel, M. Victoria, Nucl. Instrum. and Meth. B 47 (1990) 37.
[8] G. Kostorz, in: G. Kostorz (Ed.), Treatise on Materials Science and Technology, 15, Academic Press, 1982.
[9] J. Henry, M.-H. Mathon, P. Jung, J. Nucl. Mater. 318 (2003) 249.
[10] N. Baluc, R. Schäublin, P. Spätig, M. Victoria, Effects of radiation on materials, in: M.L. Grossbeck, T.R. Allen, R.G. Lott, A.S. Kumar (Eds.), 21st International Symposium, ASTM STP 1447, ASTM International, West Conshohocken, PA, 2003.
[11] A.L. Bement, in: Second International Conference on the Strength of Metals and Alloys, Conference Proceedings, vol. II, Asilomar Pacific Grove CA, USA, American Society for Metal, Metals Park, OH, USA, 1970, p. 693.